Energy-related Materials

IMR KINKEN Research Highlights 2014

Direct Molecular Dynamics Simulations of Electrocaloric Effects in Ferroelectric Materials

Using our original simulation code, "feram," we simulated the electrocaloric effect in $BaTiO_3$ directly by means of a first-principles–based, effective-Hamiltonian molecular dynamics method. The calculations were performed over a wide range of temperatures (30–900 K) and external electric fields (0–500 kV/cm). As expected, a large adiabatic temperature change was observed at the Curie temperature.

Since 2005, we have been developing our original simulation code, named "feram," specialized for ferroelectric materials. feram is a fast molecular dynamics (MD) simulation code for ABO_3 perovskite-type ferroelectrics and distributed as free software through http://loto.sourceforge.net/feram/. The code is based on a first-principles effective Hamiltonian and can be applied not only to bulk ferroelectrics but also ferroelectric thin-film capacitors. Because dipole interactions are treated in reciprocal space in the code using a fast Fourier transform (FFT), feram is fast enough to simulate ferroelectric devices with realistic system sizes up to 100 nm and over a realistic time span (> 100 ns). Using our MD simulation method, we have succeeded in constructing a phase diagram for ferroelectric thin-film capacitors subject to in-plane strain [1,2].

In 2013, we developed a method for the direct simulation of the electrocaloric effect (ECE) in ferroelectric materials with feram [3]. The ECE is an adiabatic change in the temperature, ΔT, of a material upon applying an external electric field. In particular, if an electric field is applied to a ferroelectric material at just above its phase transition temperature, T_C, and the field is then removed, a large reduction in temperature is expected. This effect has potential for applications in solid-state refrigeration technologies.

In Fig. 1, the temperature dependence of the ECE ΔT of $BaTiO_3$ under various applied initial external electric fields is compared. Even under a small initial external electric field (50 kV/cm), $BaTiO_3$ produces a large ΔT; however, the temperature range over which this large ΔT can be obtained is narrow. By increasing the applied field to levels >100 kV/cm, the range of optimal temperatures broadens.

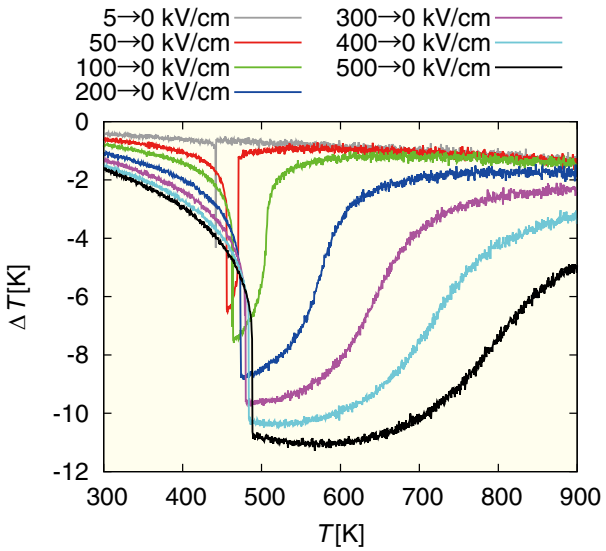

Fig. 1 The temperature dependence of ΔT for various initial applied external electric fields, E_z. The external electric field sweeps from E_z = 5-500 to E_z = 0 kV/cm.

References

[1] J. Paul, T Nishimatsu, Y. Kawazoe, and U. V. Waghmare, Phys. Rev. Lett. **99**, 077601 (2007).

[2] S. Kouser, T. Nishimatsu, and U. V. Waghmare, Phys. Rev. B **88**, 064102 (2013).

[3] T. Nishimatsu, J. A. Barr, and S. P. Beckman, J. Phys. Soc. Jpn. **82**, 114605 (2013).

Keywords: first-principles calculation, phase transition, solid-state refrigeration
Takeshi Nishimatsu (Materials Design by Computer Simulation Division)
E-mail: t-nissie@imr.tohoku.ac.jp
URL: http://t-nissie.users.sourceforge.net

Microstructural Origins of Embrittlement in Nuclear Reactor Pressure Vessel Steels

Understanding the embrittlement mechanisms in nuclear reactor pressure vessel (RPV) steels using neutron irradiation is one of the most important subjects related to the safe operation of nuclear power plants. We investigated the correlation of microstructure evolution and hardening in RPV steels using surveillance test specimens from a Finnish nuclear power reactor.

The irradiation-induced embrittlement of nuclear reactor pressure vessel (RPV) steels is a vital issue in the safe operation of nuclear power plants. Embrittlement is mainly caused by irradiation-induced changes in the microstructure, such as the formation of solute nanoclusters (SCs) and matrix damage (MD) due to irradiation-induced point defect clusters and dislocation loops. However, the details of the microstructural origins of embrittlement are not well understood. Here, we demonstrate the microstructural changes in surveillance test specimens from the Loviisa-1 reactor in Finland, which is a Russian-type pressurized water reactor (VVER-440), after initial irradiation with a neutron fluence of 2.5×10^{19} n/cm^2 (E>1 MeV), post-irradiation annealing at 475 °C for 100 hours, and re-irradiation with fluences up to 2.7×10^{19} n/cm^2 [1].

Figure 1 shows the 3D elemental maps obtained using atom probe tomography (APT). The results indicated the formation of Cu-rich SCs during the initial irradiation and their subsequent coarsening during annealing. After re-irradiation, a small number of SCs reformed.

The hardening related to the SCs was estimated using the Russell-Brown model [2] based on the APT results and was in good agreement with the measured hardening after the initial irradiation (I) and post- irradiation annealing (IA), as shown in Fig. 2. In contrast, during the re-irradiation (IAI) stage, the estimated hardening by the SCs was smaller than the measured hardening. This suggested that the hardening after re-irradiation was to the result of microstructure changes other than the SC development observed by APT. This difference was attributed to newly-formed matrix defects introduced during re-irradiation, which was supported by positron annihilation spectroscopy results [3].

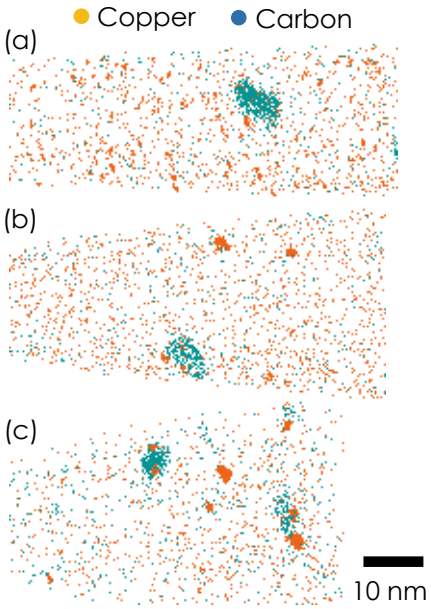

Fig. 1 Elemental distributions determined by APT in the Loviisa-1 surveillance specimens after (a) initial irradiation, (b) post-irradiation annealing, and (c) re-irradiation.

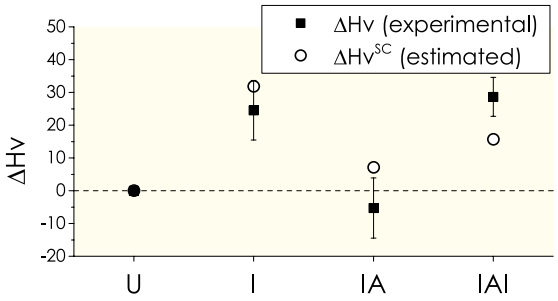

Fig. 2 Experimental values for irradiation hardening and the hardening attributed to the SCs estimated using the Russell-Brown model. U indicates the un-irradiated state.

References

[1] A. Kuramoto, T. Toyama, Y. Nagai, K. Inoue, Y. Nozawa, M. Hasegawa, and M. Valo, Acta Mater. **61**, 5236 (2013).

[2] K. Russell and L. Brown, Acta Metall. **20**, 969 (1972).

[3] T. Toyama, A. Kuramoto, Y. Nagai, K. Inoue, Y. Nozawa, Y. Shimizu, Y. Matsukawa, M. Hasegawa, and M. Valo, J. Nucl. Mater. **449**, 207 (2014).

Keywords: nuclear materials, nanocluster, radiation effects

Yasuyoshi Nagai, Koji Inoue, Yasuo Shimizu, and Kazuaki Nagumo (Irradiation Effects in Nuclear and Their Related Materials Division)
E-mail: nagai@imr.tohoku.ac.jp
URL: http://wani.imr.tohoku.ac.jp/

Damage and Recovery Processes in Luminescent Polyester Films

Polymers consisting of benzene rings are known to effectively absorb UV light, and some also exhibit photoemission in the visible region, which can be utilized for monitoring the intensity and spatial distribution of ionizing radiation. UV photon irradiation caused permanent damage to the luminescence centers in a vacuum or in an air atmosphere. In contrast, ion-induced degradation immediately recovered to a certain level when the film was exposed to air.

Popular ester compounds such as polyethylene terephthalate (PET) are luminescent and attractive for making organic scintillators for radiation measurements and preventative safety measures [1]. The optical characteristics of these materials are changed by ionizing radiation; ion bombardment of polymers induces significant chemical transformations depending on the energy deposition mechanism. Recently, we found that polyethylene naphthalate (PEN), with two benzene rings, exhibits much stronger blue luminescence in response to irradiation compared to PET [2]. The optical emission characteristics of the PEN films were drastically changed after irradiation by MeV protons and UV photons. While permanent damage was done to the photo-irradiated films, recovery of the emission properties was observed after exposure to air [3].

Photo-stimulated luminescence (PL) and ion-beam–induced luminescence (IBIL), reflected in the intensity of the two major peaks at 480 and 520 nm in the inset of Fig. 1(a), decreased with the incident fluence, particularly for ion irradiation. A lifetime analysis of PL in the PEN film indicated that the major part of the luminescence has two components at approximately 20 and 5 ns, suggesting two types of luminescence centers. During initial irradiation, the PL-intensity reduction rate in the UV-irradiated film was comparable to that for ion irradiation, but the residual PL intensity in the UV-irradiated film was considerably larger at higher fluences. In addition, no change in the PL characteristics of the UV-irradiated film was observed after stopping the UV irradiation, indicating that the damage caused by the UV photons was permanent. However, the PL intensity from the ion irradiated film recovered immediately when the film was exposed to the air. An ion-beam analysis revealed that H, C, and O atoms were released as the incident ion fluence increased. The recovery of the luminescence centers in the ion-irradiated PEN film is attributed to ion-induced surface modification, which plays a role in the enhancement of the dissociation of water molecules and the diffusion process for constituent atoms.

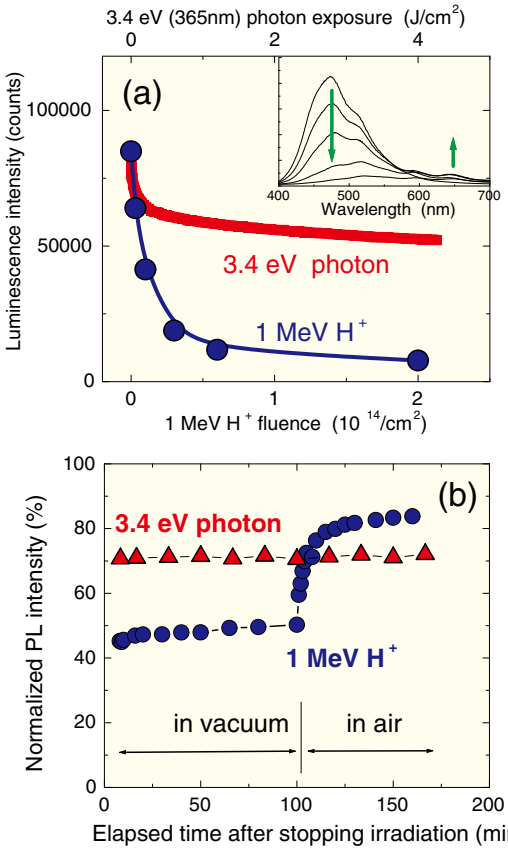

Fig 1 (a) PL spectra and intensity reduction curves at 480 nm from the PEN films irradiated by 3.4 eV photons and 1 MeV H^+ ions. (b) Time evolution of the PL intensity of the film irradiated to 5×10^{12} H^+ ions/cm^2. The sample was kept under vacuum until 100 min after stopping the ion irradiation, and then air was reintroduced into the chamber.

References

[1] S. Nagata, H. Katsui, K. Hoshi, B. Tsuchiya, K. Toh, M. Zhao, T. Shikama, and E.R. Hodgson, J. Nucl. Mater. **442** 501 (2013).

[2] S. Nagata, H. Katsui, K. Takahiro, B. Tsuchiya, and T. Shikama, Nucl. Instr. and Meth. in Phys. Res B. **268** 3099 (2010) .

[3] S. Nagata, M. Mitsuzuka, S. Onodera, T. Yaegashi, K. Hoshi, M. Zhao, and T. Shikama, Nucl. Instr. and Meth. in Phys. Res B.. **315** 157 (2013).

Keywords: luminescence, polymer, ion beam analysis
Shinji Nagata and Tatsuo Shikama (Nuclear Materials Science Division)
E-mail: nagata@imr.tohoku.ac.jp
URL: http://www-lab.imr.tohoku.ac.jp/~wshikama/

Effects of Displacive Radiation on Fe and Its Alloys

To develop materials for advanced fission and fusion reactors, we investigated the effect of radiation on Fe- and Zr-based alloys with special emphasis on modeling the microstructural evolution and the resulting changes in the mechanical properties. We developed a new method conducive to in-situ observations under irradiation in a high-voltage electron microscope (HVEM). A focused electron beam introduces an atomic displacement gradient that enhances defect diffusion in matrix. TaC and Y_2TiO_7 nanoparticles embedded in F82H and 12Cr-ODS alloys, respectively, were irradiated with electrons. The instability of the particles indicates that the diffusion of vacancies, as well as direct displacement of the constituent atoms of the particles, is attributable to these irradiation-induced dissolution phenomena.

Nanometer-scale particles embedded in steels, such as the carbides or oxides, can enhance steels' strength. When we employ these materials in nuclear reactor systems, such as fission and fusion reactors, radiation effects on the particles and their interactions with the matrix are of some concern. Irradiation-induced instability of defect clusters and particles, such as MX particles in F82H and the oxide particles in oxide dispersion-strengthened (ODS) steel, was reported recently [1, 2].

Radiation-induced defects and their underlying kinetics were first developed in high-voltage electron microscopes (HVEMs). Diffusion of matrix vacancies is enhanced both by irradiation and by vacancy concentration gradients, which are achieved solely under focused electron irradiation in an HVEM. Based on this idea, we developed a focused electron beam irradiation technique.

The basic kinetic equation is

$$\frac{dC_v(r)}{dt} = \sigma\,\phi(r) - Z_{vi}\,(M_i + M_v)\,C_i(r)\,C_v(r) - M_v C_{sv}\left(C_v(r) - C_v^0\right) + D_v \nabla^2 C_v(r)\,. \quad (1)$$

In this study, a qualitative analysis of the influence of the fourth term will be conducted using in-situ observations under irradiation conditions.

An Fe-TaC model alloy and a 9Cr-ODS steel were employed. Electron irradiation was performed in the UHVEM at Osaka University. Microstructural evolution was observed simultaneously with electron irradiation at energies ranging from 0.75 to 2.5 MeV at 673 K. The intensity of the electron beam, $\varphi(r)$, was measured using a Faraday cup.

Figure 1 and 2 shows the microstructural evolution under electron irradiation in the Fe-TaC and ODS steels. Decreases in particle size and contrast were evident. At the earliest stage of irradiation, a notable linear decrease in size was observed. The shrinkage rate was measured as a function of $\varphi(r)$ and was almost constant at high

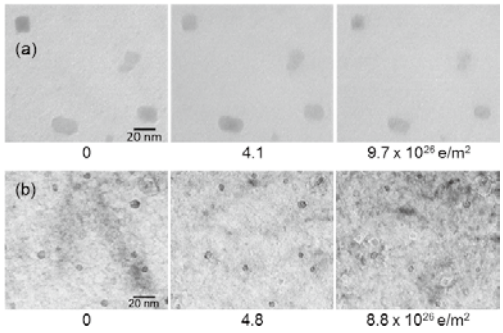

Fig. 1 Microstructural evolution in (a) Fe-TaC and (b) 9Cr-ODS irradiated with 2 MeV electrons at 673 K.

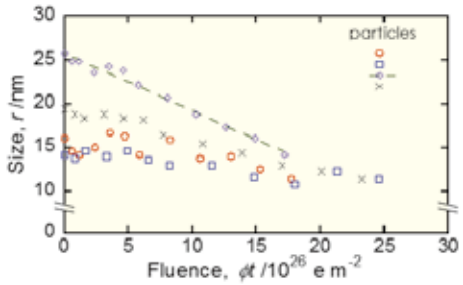

Fig. 2 Size variation of TaC particles in Fe-TaC irradiated with 2 MeV electrons at 673 K. Four representative particles are shown.

$\varphi(r)$, i.e., near the beam center. In contrast, a high shrinkage rate was obtained at lower$\varphi(r)$, i.e., in the near-vicinity of the beam, indicating the effect of the fourth term in Eq. (1). This trend was observed under irradiation by electrons with energy above 1 MeV. The shrinkage was obvious at irradiation levels higher than 1.5 MeV, while it was barely perceptible below 1 MeV. These results indicate the mechanism of instability of the embedded nanoparticles in steels under irradiation.

References

[1] H. Abe et al, Mater. Trans. **55**, 423 (2014).
[2] Y. Satoh et al, Phil. Mag. **93**, 1652 (2013).

Keywords: radiation effects, electron microscopy, mechanical properties
Hiroaki Abe and Yuhki Satoh (Nuclear Materials Engineering Division)
E-mail: abe.hiroaki@imr.tohoku.ac.jp
URL: http://www-lab.imr.tohoku.ac.jp/~abeken/

Niobium Solid Electrolytic Capacitor with Sub-micrometer Porosity Prepared by Dealloying in a Metallic Melt

Porous Nb was prepared by dealloying in a metallic melt. A Ni-Nb precursor was immersed in a Mg melt, and Ni was selectively dissolved into the melt. The remaining Nb self-organized into an interconnected structure. Removal of the Mg solvent with aqueous HNO_3 yielded open-cell sub-μm porous Nb, which was applied in solid electrolytic capacitors after anodization. The mass-specific capacitance of the anodized Nb was as high as 500,000 μFV/g and can be further increased by optimizing the dealloying conditions.

Solid electrolytic capacitors are widely used in small electronic devices because they provide large specific capacitances and unique operating characteristics at low frequency and high current. Such devices increasingly require compact and high-capacitance electrolytic capacitors, which can be achieved by increasing the relative permittivity **ε** of the dielectric layer and/or increasing the specific surface area. Nb is a promising alternative electrolytic capacitor material because of its low cost, low specific gravity, natural abundance, and the high relative permittivity of Nb_2O_5 (**ε** = 41). Conventional solid electrolytic capacitors are made by sintering sub-μm porous Nb powder into porous anodic pellets at high temperature. The size of the ligaments in the porous structure grows to the order of 1 μm such that much of the surface area in the pellet is lost during sintering. If nanoporous Nb could be prepared without sintering, the surface area and capacitance should be much improved. We recently developed a novel dealloying method using a metallic melt and fabricated three-dimensional, open-cell sub-μm porous base metals [1]. The method allows the precursor shape to be largely maintained during dealloying. Nanoporous Nb pellets can potentially be prepared directly from the precursor pellets without sintering or ligament growth. We demonstrated the preparation of high-performance solid electrolytic capacitors by this method, using high specific surface area sub-μm porous Nb [2].

Figure 1(a) shows the structure of porous Nb prepared from a Nb-Ni precursor by dealloying in Mg melt at 1123 K for 60 sec, followed by etching in HNO_3 aqueous solution to remove the Mg. It shows that sub-μm Nb particles comprise a homogeneous three-dimensional, open-cell structure. This porous Nb was anodized in 0.5 vol.% aqueous phosphoric acid at 333 K for 7 h to obtain Nb_2O_5 thin films for use as dielectric layers. Figure 1(b) shows the cyclic voltammogram for the anodized porous Nb in an electrolyte of 40 mass% aqueous H_2SO_4. The square

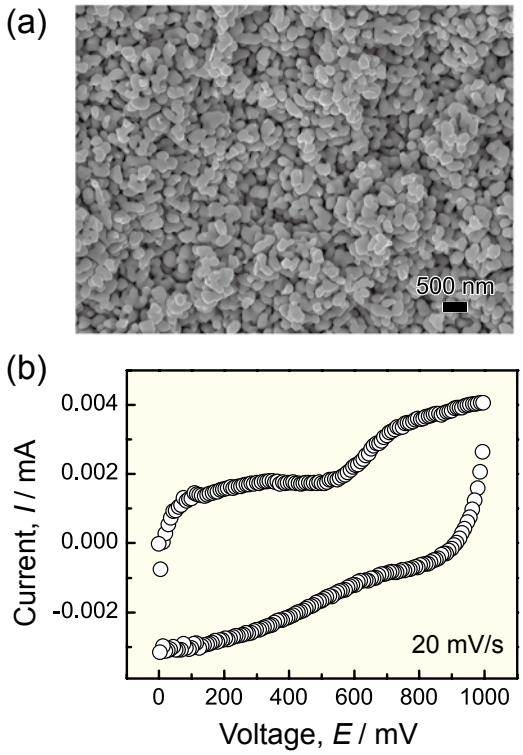

Fig.1 (a) SEM micrograph of porous Nb prepared by dealloying in Mg melt at 1123 K, for 60 s. (b) Cyclic voltammogram for the anodized porous Nb in an electrolyte of 40 mass% aqueous H_2SO_4 at 20mV/s potential sweep rate.

shape confirms that the Nb functioned as a solid electrolytic capacitor. The mass specific capacitance calculated from the area of the curve was as high as 500,000 μFV/g, and the Nb surface area was estimated to be 3.92 m^2/g. Further improvements in the capacitance of Nb solid electrolytic capacitors are expected upon optimizing dealloying conditions.

References

[1] T. Wada and H. Kato, Scripta Mater. **65**, 532 (2013)
[2] J. W. Kim, T. Wada, S. G. Kim,and H. Kato, Mater. Lett. **116**, 223 (2013)

Keywords: energy storage, porosity, nanostructure
Hidemi Kato (Non-Equilibrium Materials Division)
E-mail: hikato@imr.tohoku.ac.jp
URL: http://www.nem.imr.tohoku.ac.jp/

Sodium Fast Ionic Conduction in $Na_2B_{12}H_{12}$ Accompanied by Order-Disorder Structural Transition

We have found that the complex hydride $Na_2B_{12}H_{12}$, incorporating $[B_{12}H_{12}]^{2-}$ complex anions, exhibits sodium fast ionic conduction on the order of 0.1 S/cm above its order-disorder structural transition temperature around 530 K. The ionic conductivity may be enhanced by the large size, quasispherical shape, and high rotational mobility of the $[B_{12}H_{12}]^{2-}$ complex anions.

Complex hydrides have attracted much attention, not only as potential hydrogen storage materials but also as solid-state fast ionic conductors. Previously, we reported that $LiBH_4$ exhibits lithium fast ionic conduction, which opened up research on solid state ionics in complex hydrides [1]. We also recently worked on the design of sodium fast ionic conductors, and found that $Na_2(BH_4)(NH_2)$ shows a sodium ionic conductivity of 2×10^{-6} S/cm at room temperature because of its antiperovskite-type structure [2].

More recently, we, in collaboration with Dr. Udovic of NIST, found that $Na_2B_{12}H_{12}$, which includes $[B_{12}H_{12}]^{2-}$ complex anions, also exhibits fast ionic conduction [3]. Figure 1 (bottom) shows the temperature dependence of the ionic conductivity. The ionic conductivity increases almost log-linearly starting from the order of 10^{-7} S/cm with increasing temperature (T). Interestingly, the behavior drastically changes at approximately 530 K; the conductivity jumps by nearly 3 orders of magnitude to reach the order of 0.1 S/cm.

This significant increase in the ionic conductivity is attributed to the order-disorder structural transition. As shown in Fig. 1 (top), the crystal structure of $Na_2B_{12}H_{12}$ changes from monoclinic to body-centered cubic (bcc) at about 530 K. During this first-order structural transition, the quasispherical, icosahedral $[B_{12}H_{12}]^{2-}$ complex anions undergo bcc packing with significant orientational disorder, represented schematically by a variety of superimposed orientations. In contrast to the fully-occupied cation sites of the monoclinic ordered structure, the Na^+ cations in the bcc structure are disordered among a complex sublattice of off-center sites within the relatively large, distorted tetrahedral interstices of the complex anions. Besides the presence of cation vacancies, the anion/cation size ratio is also a key factor influencing the conductivity since larger anions lead to enlarged interstitial diffusion pathways.

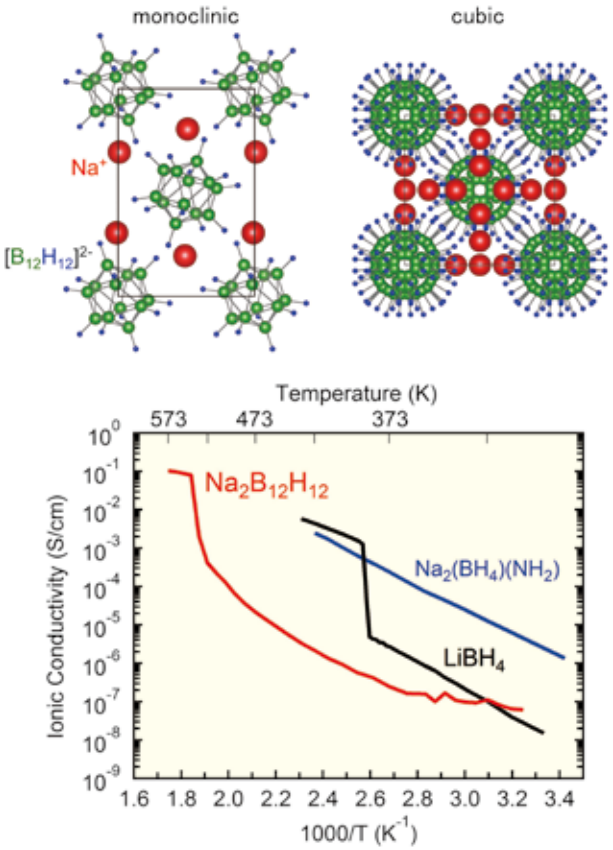

Fig. 1 (top) Crystal structures of the low-temperature ordered monoclinic and high-temperature disordered cubic $Na_2B_{12}H_{12}$. (bottom) Temperature dependence of the ionic conductivity of $Na_2B_{12}H_{12}$ compared with that for other complex hydride.

References

[1] M. Matsuo and S. Orimo, Adv. Energy Mater. **1**, 161 (2011).
[2] M. Matsuo, S. Kuromoto, T. Sato, H. Oguchi, H. Takamura, and S. Orimo, Appl. Phys. Lett. **100**, 203904 (2012).
[3] T.J. Udovic, M. Matsuo, A. Unemoto, N. Verdal, V. Stavila, A.V. Skripov, J.J. Rush, H. Takamura, and S. Orimo, Chem. Comm. **50**, 3750 (2014).

Keywords: ionic conductor, energy storage
Motoaki Matsuo and Shin-ichi Orimo (Hydrogen Functional Materials Division)
E-mail: mmatsuo@imr.tohoku.ac.jp, orimo@imr.tohoku.ac.jp
URL: http://www.hydrogen.imr.tohoku.ac.jp/

Development of Fe-Co Alloy Thin Films for Vibration Energy-Harvesting Systems

Magnetostrictive materials are promising candidates for use in magnetomechanical conversion applications such as actuators, sensors, and vibration energy-harvesting devices, a renewable energy technology. We enhanced the magnetostrictive properties of a rare-earth–free Fe-Co alloy thin film by controlling the microstructure. Here, we highlight the features of these materials and the challenges to their application in vibration energy-harvesting devices.

In recent years, a strong interest in introducing magnetostrictive thin films into microelectromechanical systems (MEMS) as novel actuators, sensors, and vibration energy-harvesting devices has developed. Rare-earth–based magnetostrictive materials, represented by Tb-Dy-Fe, have played a central role in the development of applications owing to their large magnetostriction capabilities. However, there has also been a demand for rare-earth–free magnetostrictive materials. In this report, we summarize our recent work on the development of Fe-Co alloy thin films.

Figure 1 shows the annealing-temperature dependence of the saturation magneto- striction of $Fe_{32}Co_{68}$ alloy thin films sputter-deposited on a quartz glass substrate. As the annealing temperature increased, the saturation magnetostriction increased, reaching a maximum of 159 ppm at 1073 K, which is almost three times larger than that of the sample annealed at 673 K. We also observed an increase in the magnetization at the grain boundaries of Fe-Co alloy thin films with large magnetostriction, as seen in the inset of Fig. 1, which suggest the strong magnetostrictive effect originates from the heterogeneity that develops at the phase boundaries in the Fe-Co alloys.

Figure 2 shows a photograph of a vibration energy harvesting device comprised of an Fe-Co alloy thin film developed in this study and a winding wire. This device can generate small quantities of electric power from environmental vibrations. This technology has could lead to novel self-powering applications that do not require a traditional power supply (such as a battery), which can only deliver electric power for limited durations.

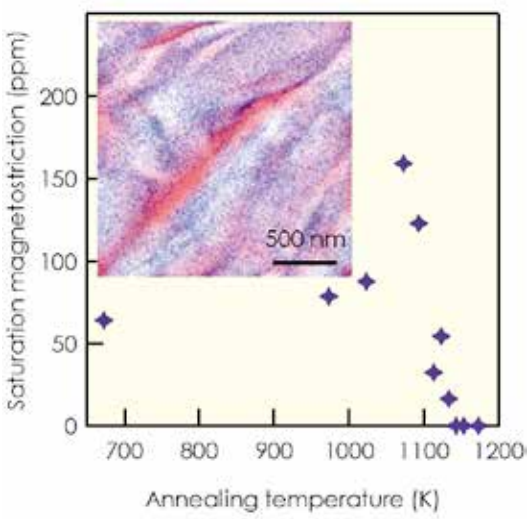

Fig. 1 Annealing-temperature dependence of the saturation magnetostriction of Fe-Co alloy thin films. The inset shows superimposed AFM (red) and MFM (blue) images.

Fig. 2 Vibration-energy–harvesting device incorporating an Fe-Co alloy thin film.

References

[1] T. Nakajima, T. Takeuchi, I. Yuito, K. Kato, M. Saito, K. Abe, T. Sasaki, T. Sekiguchi, and S. Yamaura, Mater. Trans., **55**, 556 (2014).

Keywords: magnetic properties, alloy, energy storage

Takashi Nakajima and Shin-ichi Yamaura (Advanced Materials Development and Integration of Novel Structured Metallic and Inorganic Materials)
E-mail: tnakajima@imr.tohoku.ac.jp
URL: http://amdi-pro.imr.tohoku.ac.jp/en/index.html